Soft Matter

PAPER

View Article Online
View Journal | View Issue

Published on 02 March 2020. Downloaded by National Synchrotron Radiation Research on 1/27/2021 3:24:05 AM.

Check for updates

Cite this: *Soft Matter*, 2020, **16**, 3505

Correlations between temperature-dependent rheology and electrostatic interactions in reverse wormlike micelles induced by inorganic salts†

Hung-Ming Chang,‡ Chia-Yi Lin‡ and Shih-Huang Tung *

Received 23rd December 2019,
Accepted 1st March 2020

DOI: 10.1039/c9sm02508a

rsc.li/soft-matter-journal

Previous studies have shown that the plateau modulus G_p of the wormlike micelles formed in water driven by hydrophobic interactions is a constant upon heating, similar to polymer solutions, and G_p of the reverse worms formed in oils driven by hydrogen bonding decreases with increasing temperature. In this work, we investigated the reverse worms induced by three chloride salts that bind lecithin through different strengths of electrostatic interactions, in the order of $LaCl_3$ > $CaCl_2$ > LiCl. We correlated the interaction strengths with the temperature-dependent rheological properties and found that upon heating, G_p for all the reverse worms driven by electrostatic interactions decays slower than that driven by the weak temperature-sensitive hydrogen bonding. Furthermore, the decay rates of G_p follow an order in the inverse relation to the interaction strength, $LaCl_3$ ≤ $CaCl_2$ < LiCl, indicating that the dependence of G_p on temperature can reflect the strength of the driving forces for micellization. We utilized Fourier transform infrared spectroscopy (FTIR) to confirm the weakening of the interaction and the small angle X-ray scattering (SAXS) technique to reveal the decrease in the lengths of the reverse worms as temperature increases, both of which echo the changes in the rheological properties.

1. Introduction

Wormlike micelles are flexible cylindrical chains with radii in the nanometer scale and contour lengths up to several microns,[1,2] which are self-assembled by surfactants with distinct hydrophilic and hydrophobic portions either in water or in low-polar organic solvents (oils).[3–6] The hydrophilic surfactant heads of the "normal" wormlike micelles formed in water face outward to come into contact water and shield the hydrophobic tails in the interior of the micelle. "Reverse" or "inverted" wormlike micelles formed in low-polar organic solvents have the opposite structure, with the tails swelling in the solvents and the heads buried in the core of the micelle. In water, the self-assembly is mainly driven by the hydrophobic interaction,[7,8] while in low-polar organic solvents, it is the specific interactions between the hydrophilic components in the micellar core that trigger the self-assembly, such as hydrogen bonds or electrostatic attractions.[9,10]

The rheological behaviors of normal and reverse worms are generally considered to be analogous.[8] They are similar to polymer chains in their ability to entangle into viscoelastic networks above a semidilute threshold.[1] However, unlike polymer chains that are firmly linked by covalent bonds, surfactants exchange between micelles. The wormlike chains can break and recombine because they are held by weak physical bonds.[11] The rapid breaking and recombination process compared to the reptation of chains gives rise to the characteristic Maxwellian rheological response with a single relaxation time.[4,8] Recently, a key difference between normal and reverse worms with respect to how their rheological properties change upon heating has been reported.[12] For normal worms in water, the plateau modulus G_p remains constant and the relaxation time t_R exponentially decays as temperature increases. For the lecithin/water or lecithin/bile salt reverse worms that are driven by hydrogen bonding, both G_p and t_R decrease exponentially upon heating. As a result, the zero-shear viscosity η_0 of reverse worms decreases more rapidly with temperature than that of normal worms, consistent with the predication of the $\eta_0 \approx G_p t_R$ relationship. Such a contrasting effect is attributed to the fact that the hydrophobic interaction is temperature-insensitive while hydrogen bonds decay exponentially with temperature.[9,13] A more rapid decrease in the contour length of chains thus occurs for the reverse worms driven by hydrogen bonding upon heating.

Lecithin (Fig. 1) is a class of lipids frequently used for preparing reverse wormlike micellar solutions. Apart from the reverse worms induced by water or bile salts through hydrogen

Institute of Polymer Science and Engineering and Advanced Research Center for Green Materials Science and Technology, National Taiwan University, Taipei 10617, Taiwan. E-mail: shtung@ntu.edu.tw

† Electronic supplementary information (ESI) available. See DOI: 10.1039/c9sm02508a

‡ These authors contributed equally to this study.

Published on 02 March 2020. Downloaded by National Synchrotron Radiation Research on 1/27/2021 3:24:05 AM.

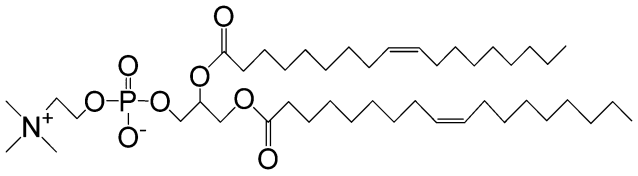

Fig. 1 Molecular structures of lecithin used in this study.

bonds,[14] it has been reported that the addition of inorganic salts with specific divalent and trivalent cations, such as Ca^{2+} and La^{3+},[10,15] can transform lecithin spherical micelles into cylindrical ones that are sufficiently long and robust to cause gelation, which is driven by the electrostatic interactions between the ions and the zwitterionic lecithin headgroups.[15] Most of the lecithin/inorganic salt systems show gel-like behaviors instead of typical Maxwell viscoelastic response at room temperature, possibly because the strong electrostatic attractions suppress the breaking/recombination process of the unusually long micellar chains.[2,8,12] Later on a study dealing with the effect of monovalent alkali halides demonstrated that the binding strength of the alkali cations with lecithin is in the order of $Li^+ > Na^+ > K^+$ and more importantly, the cation–lecithin interaction is affected by the paired halide anions following the order $I^- > Br^- > Cl^-$.[16–19] Although the electrostatic interactions between monovalent cations and lecithin are weaker than those for multivalent ones, the monovalent salts of relatively stronger interactions with lecithin, including LiCl, LiBr, LiI and NaI, can indeed induce organogels. In other words, the strength of the electrostatic interaction and the ability to induce reverse worms are highly ion-dependent.

The electrostatic interactions are temperature-sensitive and generally stronger than hydrogen bonding.[20] Along with the tunable strengths by varying ions, the lecithin/inorganic salt systems provide a good platform to investigate the effect of temperature on the rheological properties of micellar solutions. The results can be compared to those induced by the temperature-insensitive hydrophobic interactions and the highly temperature-sensitive hydrogen bonding. In this work, we focus on three inorganic salts, lanthanum chloride ($LaCl_3$), calcium chloride ($CaCl_2$), and lithium chloride (LiCl), all of which are chloride salts so as to rule out the effects of anions. The salts can induce lecithin organogels at room temperature but the ability is different, in the order of $LaCl_3 \geq CaCl_2 >$ LiCl, consistent with the valences of the cations.[15,16,18] Upon heating, the organogels are transformed into viscoelastic fluids and then low-viscosity liquids. For a comparison with other viscoelastic micellar solutions, we studied the rheology in the temperature windows where the solutions show viscoelasticity in the dynamic rheological tests so that G_p, t_R, and η_0 can be successfully extracted from the data. We compare the changes in the rheological parameters with increasing temperature for the reverse worms driven by different strengths of electrostatic interactions. The changes in the radius and the length of the reverse worms upon heating were determined by SAXS and the interaction strengths were probed by FTIR to build the relationship among the molecular interaction, rheological properties, and micellar structure.

2. Experimental section

2.1 Materials

Inorganic salts, $LaCl_3$, $CaCl_2$, and LiCl (all with 99.99% purity), and *n*-decane (99%) were purchased from Sigma-Aldrich. The zwitterionic phospholipid, soybean lecithin (95%), was purchased from Avanti Polar Lipids, Inc. All chemicals were used as received.

2.2 Sample preparation

Lecithin/inorganic salt reverse wormlike micelles in *n*-decane were prepared by a procedure similar to that described in our earlier articles.[11,15,16] First, lecithin and inorganic salts were dissolved separately in methanol to form 100 mM stock solutions, respectively. Samples of the desired composition were prepared by mixing the stock solutions. Methanol was removed in a vacuum oven at 55 °C for 48 h, which also ensured the removal of residual water from the samples. The final samples with desired concentrations were obtained by adding *n*-decane, followed by stirring until the solutions became homogeneous and transparent. All samples were equilibrated at room temperature at least 5 days prior to experiments.

2.3 Rheology

Steady and dynamic rheological experiments were performed on an AR2000ex stress-controlled rheometer (TA Instruments) using parallel-plate geometry with Peltier temperature control. A solvent trap was used to minimize solvent evaporation. The samples were equilibrated for at least 10 min at each temperature before measurements. Frequency spectra were recorded in the linear viscoelastic regime of the samples, as determined from dynamic strain sweep tests. For the steady-shear experiments, sufficient time was allowed before data collection at each shear rate, ensuring that the viscosity reached the steady-state value.

2.4 FTIR

FTIR spectra were recorded in the transmission mode with a Spectrum 100 model FTIR spectrometer (PerkinElmer). Samples of 40 mM lecithin with varying molar ratios of salts in *n*-decane were loaded into a KBr liquid cell (0.05 mm thickness) and analyzed over a range of wavenumbers from 4000 to 450 cm^{-1} at different temperatures. The samples were equilibrated at least 10 min at each temperature. Each spectrum was collected under an accumulation of 16 scans at 4 cm^{-1} resolution. Pure solvent in the KBr cell was taken as the background reference.

2.5 SAXS

SAXS measurements were conducted on the BL23A1 beamline in the National Synchrotron Radiation Research Center (NSRRC), Taiwan,[21] with a monochromatic beam of wavelength λ = 0.83 Å.

 This journal is © The Royal Society of Chemistry 2020

Published on 02 March 2020. Downloaded by National Synchrotron Radiation Research on 1/27/2021 3:24:05 AM.

The scattering patterns were collected on a Pilatus 1M-F detector over a wave vector q range from 0.01 to 0.4 Å^{-1} at different temperatures. The spectra are shown as plots of the absolute intensity I *versus* the wave vector $q = 4\pi \sin(\theta/2)/\lambda$, where θ is the scattering angle.

2.6 SAXS modeling

Modeling of SAXS data was conducted using the package provided by NIST.[22–25] For dilute solutions of non-interacting scatterers, the scattering intensity $I(q)$ can be exclusively modeled by the form factor $P(q)$ of the scatterers

$$I(q) = cP(q) + B \quad (1)$$

where c is the total concentration of scatterers and B is the background. In this study, the form factor for a cylinder with polydisperse length was used and is given by

$$P(q) = (\Delta\rho)^2(\pi R_c^2 L)^2 \int_0^{\pi/2} [F(q,\alpha)]^2 \sin\alpha \mathrm{d}\alpha \quad (2)$$

$$F(q,\alpha) = \frac{J_1(qR_c \sin\alpha)}{(qR_c \sin\alpha)} \cdot \frac{\sin(qL\cos\alpha/2)}{(qL\cos\alpha/2)} \quad (3)$$

where $\Delta\rho$ is the difference in scattering length density between the scatterer and the solvent, L is the length, R_c is the radius of the cylinder, and α is the angle between the wave vector q and the cylinder axis. $J_1(x)$ is the first-order Bessel function of the first kind, given by

$$J_1(x) = \frac{\sin x - x\cos x}{x^2} \quad (4)$$

For the cylinders with polydisperse length, the form factor is averaged over the length distribution as follows

$$P(q) = \int f(L) \cdot P(q,L)\, \mathrm{d}L \quad (5)$$

where $P(q, L)$ is the form factor for the cylinder of length L and Schulz distribution is used to describe the polydispersity of cylinder length $f(L)$:

$$f(L) = \left(\frac{z+1}{L_0}\right)^{z+1} \frac{L^z}{\Gamma(z+1)} \exp\left(-(z+1)\frac{L}{L_0}\right) \quad (6)$$

where L_0 is the average cylinder length, Γ is the gamma function, and z is a parameter related to the width of the distribution. The polydispersity index p_d is defined by

$$p_d = \frac{1}{\sqrt{z+1}} \quad (7)$$

3. Results and discussion

We first examined the interaction strengths between lecithin and the three inorganic salts by FTIR at room temperature. The molar ratio of an inorganic salt to lecithin is defined as S_0. Fig. 2 shows the absorption bands of the phosphate group (PO_4^-) on lecithin without and with the inorganic salts at the same S_0 = 0.31. The band in the presence of water in the same ratio is also displayed for a comparison. The concentration of lecithin is 40 mM. Pure lecithin shows a phosphate absorption band at 1262 cm^{-1} and the band redshifts to 1215, 1251, 1257 and 1260 cm^{-1} for $LaCl_3$, $CaCl_2$, LiCl, and H_2O, respectively. The higher redshift indicates a stronger interaction between the additives and lecithin. Therefore, the electrostatic interactions are stronger than the hydrogen bonding between water and lecithin, and the electrostatic interaction strength is in the order of $LaCl_3$ > $CaCl_2$ > LiCl. The higher valent cations show a higher binding strength to the negatively charged phosphate on the lecithin headgroup. It has been reported that the S_0 ranges for the formation of highly viscous or gel-like solutions are above 0.25, 0.25, and 0.60 for $LaCl_3$, $CaCl_2$, and LiCl, respectively.[15,16] For an effective comparison of the rheological parameters, including G_p, t_R, and η_0, we chose the specific S_0 and concentrations that allow the lecithin/inorganic salt mixtures in *n*-decane to exhibit viscoelastic behaviors between 25 and 40 °C, *i.e.*, the crossovers of elastic modulus G' and viscous modulus G'' can be observed in the frequency sweep tests. The temperature-dependent SAXS and FTIR data corresponding to the rheological changes were then collected and discussed.

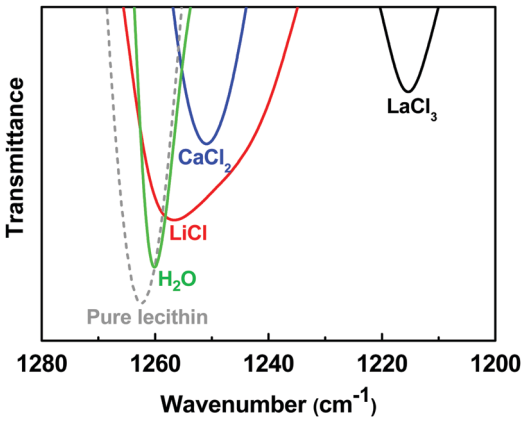

Fig. 2 FTIR absorption bands of phosphate groups on lecithin in the presence of inorganic salts and water in *n*-decane at room temperature. The molar ratios of additives to lecithin (S_0) for all the mixtures are fixed at 0.31.

3.1 Temperature effects on dynamic rheology

Fig. 3 compares the dynamic rheological data for the three inorganic salts at varying temperatures. The concentration of lecithin is 80 mM and S_0s are 0.31, 0.31, and 0.75 for $LaCl_3$, $CaCl_2$, and LiCl, respectively, which are far below the phase separation threshold for each salt. Fig. 3a–c shows G' and G'' as functions of frequency at four representative temperatures where the solutions all behave as viscoelastic fluids. As the temperature increases, the whole G' and G'' spectra of LiCl move downward and their crossovers move to higher frequency (shorter timescales), whereas in the cases of $LaCl_3$ and $CaCl_2$, the crossovers nearly horizontally shift to higher frequency and their G' and G'' spectra at different temperature converge at high frequency. The G' and G'' spectra of the LiCl sample are apparently more sensitive to temperature.

Published on 02 March 2020. Downloaded by National Synchrotron Radiation Research on 1/27/2021 3:24:05 AM.

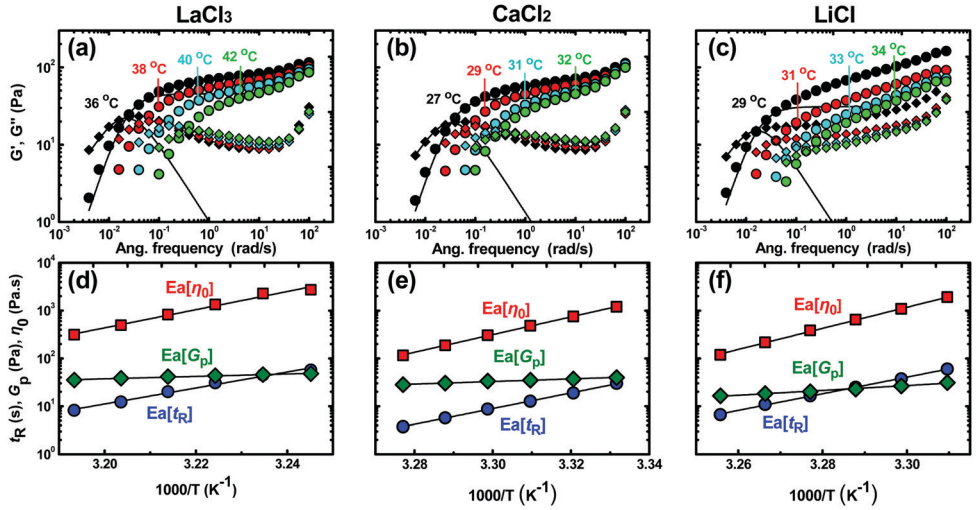

Fig. 3 (a–c) Dynamic rheology at different temperatures for lecithin/inorganic salt mixtures. The elastic modulus G' (circles) and the viscous modulus G'' (diamonds) are shown as functions of frequency ω. The solid lines are fits to the single-relaxation-time Maxwell model. (d–f) Arrhenius plots of G_p, t_R, and η_0 as functions of $1/T$ for the mixtures.

G's in Fig. 3a–c approximately reach plateaus at high frequency and the slopes of G' and G'' are close to 2 and 1, respectively, at low frequency. Such rheological behaviors can be reasonably described by the single-relaxation-time Maxwell model given by[8,26]

$$G'(\omega) = \frac{G_p \omega^2 t_R^2}{1 + \omega^2 t_R^2} \quad (8)$$

$$G''(\omega) = \frac{G_p \omega t_R}{1 + \omega^2 t_R^2} \quad (9)$$

Here G_p is the plateau modulus, *i.e.* the value of G' in the high-frequency limit, and t_R is the relaxation time of the micellar chains that can be estimated as $1/\omega_c$, where ω_c is the frequency at which G' and G'' intersect. The variations of G_p and t_R with temperature can then be determined by fitting the G' and G'' data to the Maxwell model. The representative fits are shown as the solid curves through the data at the lowest temperature for each salt in Fig. 3a–c. The fits to all the temperatures of the three salts can be found in Fig. S1–S3 of the ESI.† The semilog plots of G_p and t_R *vs.* $1/T$ are shown in Fig. 3d–f which also include the dependence of η_0 on temperature determined from the steady-shear tests. The viscosity data for the three salts from the steady-shear tests are shown in Fig. S4 of the ESI.† All the rheological parameters fall on straight lines. t_R and η_0 decay with temperature, as expected. Different from the temperature-insensitive G_p of the polymer solutions with covalently bonded chains and the aqueous wormlike micellar solutions driven by the hydrophobic interaction, the reverse worms driven by electrostatic interactions show a decrease in G_p upon heating.

The dependences of t_R and η_0 on temperature for molecules in solutions are generally expressed in the following Arrhenius form that can fit the straight lines in the semilog plots,[27,28]

$$t_R = A_t \exp\left(\frac{E_a[t_R]}{RT}\right) \quad (10)$$

$$\eta_0 = A_\eta \exp\left(\frac{E_a[\eta_0]}{RT}\right) \quad (11)$$

where $E_a[t_R]$ and $E_a[\eta_0]$ are the activation energies, *i.e.* the energy barriers for micellar chain sliding past one another, A_t and A_η are the pre-exponential factors, and R is the gas constant. According to the Maxwell fluid relationship $\eta_0 \approx G_p t_R$, $E_a[t_R]$ and $E_a[\eta_0]$ should be approximately the same if G_p is insensitive to temperature and can be assumed a constant. However, $E_a[t_R]$s determined from the slopes in Fig. 3d–f are 139.1, 136.0, and 144.4 kJ mol^{-1} and $E_a[\eta_0]$s are larger, 157.9, 154.0, and 185.0 kJ mol^{-1} for $LaCl_3$, $CaCl_2$, and LiCl, respectively. In other words, η_0 decreases more rapidly than does t_R with temperature for all the salts. Since G_p drops linearly with $1/T$, we also use the Arrhenius form to express the dependence of G_p on temperature[1]

$$G_p = A_G \exp\left(\frac{E_a[G_p]}{RT}\right) \quad (12)$$

$E_a[G_p]$s determined from the slopes are 21.0, 22.6, and 42.2 kJ mol^{-1} for $LaCl_3$, $CaCl_2$, and LiCl, respectively. The values of $E_a[\eta_0]$, $E_a[G_p]$, and $E_a[t_R]$ agree well with the Maxwell fluid relationship for all the salts, following the exponential rule, $E_a[\eta_0] = E_a[G_p] + E_a[t_R]$, as summarized in Table 1, even though G_p is not a constant with temperature. Interestingly, the decay rate of G_p upon heating is in the inverse order of the effectiveness of the salts to induce gelation, *i.e.*, $LaCl_3 \leq CaCl_2 <$ LiCl. Note that the $E_a[G_p]$s for the reverse worms driven by the electrostatic interactions are smaller than those driven by the weaker hydrogen bonding as reported previously ($\sim$53 kJ mol^{-1}),[12] implying that $E_a[G_p]$ can reflect the strength of the driving force for the reverse self-assembly.

 This journal is © The Royal Society of Chemistry 2020

Published on 02 March 2020. Downloaded by National Synchrotron Radiation Research on 1/27/2021 3:24:05 AM.

Table 1 Activation energy E_a of the rheological parameters for the reverse worms induced by the three inorganic salts in *n*-decane

Salts	[salt]/[lecithin] (mM/mM)	$E_a[G_p]$ (kJ mol^{-1})	$E_a[t_R]$ (kJ mol^{-1})	$E_a[\eta_0]$ (kJ mol^{-1})
$LaCl_3$	24.8/80 = 0.31	21.0 ± 1.3	139.1 ± 7.4	157.9 ± 8.9
$CaCl_2$	24.8/80 = 0.31	22.6 ± 1.2	136.0 ± 1.8	154.0 ± 1.6
LiCl	60/80 = 0.75	42.2 ± 2.3	144.4 ± 21.3	185.0 ± 4.8

The average micellar length $\bar{L}$ can be quantitatively determined by the dynamic rheological properties following the formula[29–32]

$$\frac{l_e}{L} \approx \frac{G_{min}''}{G_p} \quad (13)$$

where G_{min}'' is the loss modulus at its local minimum, which occurs at relatively high frequency where G' nearly reaches the plateau modulus G_p, l_e is the average length between two entanglement points, which is correlated with G_p as[31]

$$G_p \approx \frac{kT}{l_e^{9/5} l_p^{6/5}} \quad (14)$$

where l_p is the persistence length that is assumed to be 15 nm, a normal length for micellar chains,[6] k is Boltzmann's constant. We calculated $\bar{L}$s of the $LaCl_3$ and $CaCl_2$ samples at varying temperature where the G_{min}''s can be extracted from the frequency sweep curves, as listed in Table S1 of the ESI.† As temperature increases, $\bar{L}$ of the $LaCl_3$ sample decreases from 5024 Å at 36 °C to 3620 Å at 41 °C while that of the $CaCl_2$ sample decreases from 4658 Å at 27 °C to 3127 Å at 32 °C. $\bar{L}$ is predicted to decrease exponentially with temperature according to the equation[1]

$$\bar{L} \approx \phi^{1/2} \exp\left(\frac{E_c}{2kT}\right) \quad (15)$$

Here, ϕ is the volume fraction of worms, E_c is the end-cap energy, *i.e.*, the excess energy associated with the hemispherical caps compared to the cylindrical body of the worm. The slopes of $\ln\bar{L}$ *vs.* $1/T$ determined using eqn (15) are 2.7 ± 0.3 and 3.3 ± 0.2 for $LaCl_3$ and $CaCl_2$, respectively, which shows a slower decay in length for the $LaCl_3$ sample, consistent with its less temperature-dependent G_p.

The dependence of G' on temperature can be even clearly seen in Fig. 4 which shows G' normalized by the modulus at 25 °C (G_0') as a function of temperature for the three inorganic salts measured at 20 rad s^{-1} frequency with a heating rate at 2 °C min^{-1}. The samples are in the same compositions as those shown in Fig. 3. The $LaCl_3$ sample nearly maintains its G' until softening occurs around 45 °C while G' of the LiCl sample monotonically decreases in the highest decay rate upon heating. The resistance to thermal softening for the solutions correlates with the interactions between the salts and lecithin, *i.e.*, $LaCl_3$ > $CaCl_2$ > LiCl. There is a considerable difference in the temperature-dependent G'/G_0' between the divalent and trivalent cations in this test though the difference is not as obvious in the change in G_p with temperature as described above.

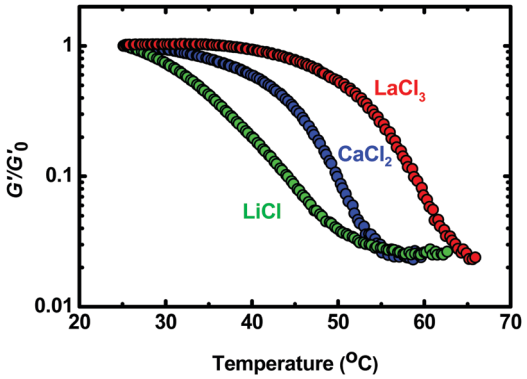

Fig. 4 Normalized elastic moduli of the lecithin/inorganic salt mixtures tested at 20 rad s^{-1} in the temperature ramp mode with a heating rate of 2 °C min^{-1}.

3.2 Temperature effects on micellar structures by SAXS

We then utilized SAXS to investigate the structural evolution of the reverse worms with increasing temperature. The S_0s for the samples were the same as those for the rheological tests. The lecithin concentration of the samples was fixed at a relatively low value of 40 mM to eliminate the scattering contributed from the structure factor caused by intermicellar interactions. The SAXS spectra at temperatures between 25 and 65 °C for the three salts are shown in Fig. 5. All the curves show slopes close to 1 at intermediate q, characteristic of cylindrical micelles that can be long and entangled to enhance the solution viscosity. The downturn region around $q \sim 0.1$ Å^{-1} provides information about the cross-sectional sizes of the cylinders and the intensity at the low q region of the scattering data is related to the lengths of the cylinders. Upon heating, the positions of the downturns are nearly unchanged for all the salts, indicating that the radii of the cylinders are not affected by temperature. In the low q region, the slopes of the scattering intensities of the $LaCl_3$ sample are almost the same as the temperature increases, whereas those of the $CaCl_2$ and LiCl samples significantly decrease above 65 °C and 55 °C, respectively, implying a greater decrease in the length of the worms, especially for LiCl. The overlapped SAXS profiles at different temperatures for each salt are shown in Fig. S5 of the ESI,† which can more clearly show that the decrease in the slope with increasing temperature in the low-q range is in the order of $LaCl_3$ < $CaCl_2$ < LiCl. The SAXS data show that the lengths of cylindrical micelles driven by weaker interactions are more sensitive to temperature.

We further used the cylinder model with polydisperse length (eqn (1)–(7)) to fit the scattering data, shown as the solid curves through the SAXS data in Fig. 5. The radii R_cs and the average

Published on 02 March 2020. Downloaded by National Synchrotron Radiation Research on 1/27/2021 3:24:05 AM.

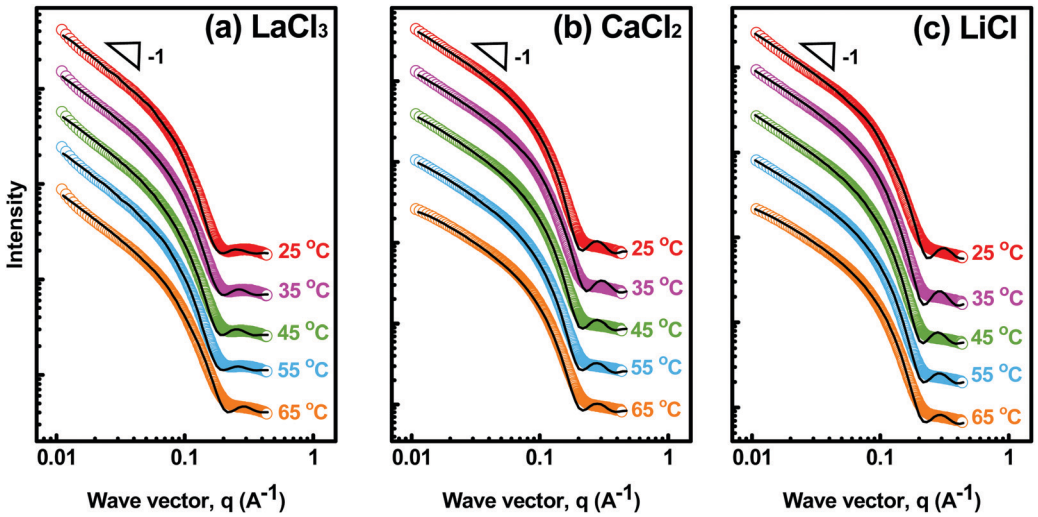

Fig. 5 SAXS data for lecithin/inorganic salt mixtures in *n*-decane at varying temperature.

Table 2 Average length L_0 and radius R_c of the reverse worms at varying temperature from SAXS modeling

	$LaCl_3$		$CaCl_2$		LiCl	
Temperature (°C)	L_0 (Å)	R_c (Å)	L_0 (Å)	R_c (Å)	L_0 (Å)	R_c (Å)
25	1709.5 ± 9.0	19.4	1405.3 ± 19.8	18.2	1493.6 ± 16.4	18.5
35	1709.3 ± 3.0	19.3	1401.6 ± 18.9	18.2	1308.6 ± 13.8	17.4
45	1708.3 ± 4.1	19.6	1397.4 ± 13.9	18.0	1193.3 ± 36.8	17.7
55	1707.4 ± 9.2	19.4	1393.1 ± 14.5	18.1	453.1 ± 10.7	17.5
65	1706.3 ± 1.2	18.3	902.8 ± 25.3	18.1	265.7 ± 5.1	17.2

lengths L_0s of the reverse worms are listed in Table 2. The radii of the cylinders for the three salts are indeed independent of temperature. However, we notice that the radius of the $LaCl_3$-induced worms is ~19 Å, larger than those of the $CaCl_2$- and LiCl-induced worms, ~17–18 Å. This could be due to the stronger $LaCl_3$–lecithin interaction that causes a more straightened conformation of lecithin molecules in reverse worms.[33–35] The lengths of the cylinders from the modeling for the $LaCl_3$ worms are nearly constant upon heating, ~1700 Å. In contrast, the lengths of the $CaCl_2$ worms decrease from ~1400 Å to 902.8 Å at 65 °C and those of the LiCl worms greatly decrease from 1493.6 Å at room temperature to 453.1 Å at 55 °C and 265.7 Å at 65 °C. The less temperature-dependent length measured with SAXS for $LaCl_3$ is in good agreement with $\bar{L}$ estimated by the dynamic rheology shown in Table S1 (ESI†). Note that the q range in the experiments is not low enough to provide the real contour lengths of the reverse worms. The length of the SAXS modeling here can only reflect the dependence of the large-scale part of the cylinders on temperature and it indeed confirms that the LiCl worms are more vulnerable to heat, consistent with the trend of the rheological properties.

3.3 Temperature-dependent interactions by FTIR

The interactions between inorganic salts and lecithin, *i.e.* the driving forces for the reverse self-assembly, should be the key to dictate the micellar structures and the rheological properties of the reverse worms. It has been shown that the primary site on lecithin to bind the salts, specifically the cations, is the negatively charged phosphate group.[15,16] Here we used FTIR to probe the temperature-dependent interactions between inorganic salts and the phosphate on the lecithin headgroup. The FTIR spectra for the phosphate stretching band affected by the three inorganic salts are shown in Fig. 6. The lecithin concentration is 40 mM in *n*-decane and S_0s are the same as those in the rheological tests, *i.e.*, 0.31, 0.31, and 0.75 for $LaCl_3$, $CaCl_2$, and LiCl, respectively. The phosphate bands in the presence of salts at 25 °C redshift to 1215, 1251, and 1237 cm^{-1} for $LaCl_3$, $CaCl_2$, and LiCl, respectively, from 1262 cm^{-1} of pure lecithin. The corresponding degrees of redshift ($\Delta\nu_{salt}$) are 47, 11, and 25 cm^{-1}. In comparison with Fig. 2 where S_0 is fixed at 0.31 for all the salts, the larger redshift of the LiCl sample than that of the $CaCl_2$ one here is due to its higher S_0 (0.75) that is required to induce viscoelastic behaviors. The shifts of the absorption bands are summarized in Table 3.

As temperature increases, the phosphate bands of lecithin in the mixtures gradually move back to higher wavenumbers and approach the band of pure lecithin for all the salts, *i.e.*, a blueshift that implies weakening of interactions between cations and phosphate. At 75 °C, the bands shift to 1217, 1252, and 1241 cm^{-1} for $LaCl_3$, $CaCl_2$, and LiCl, respectively. The degrees of blueshift from 25 to 75 °C ($\Delta\nu_{25\rightarrow75}$) for the three salts are 2, 1, and 4 cm^{-1}. A significant blueshift can be seen for LiCl even though its S_0 is the highest. For a better comparison

 This journal is © The Royal Society of Chemistry 2020

Published on 02 March 2020. Downloaded by National Synchrotron Radiation Research on 1/27/2021 3:24:05 AM.

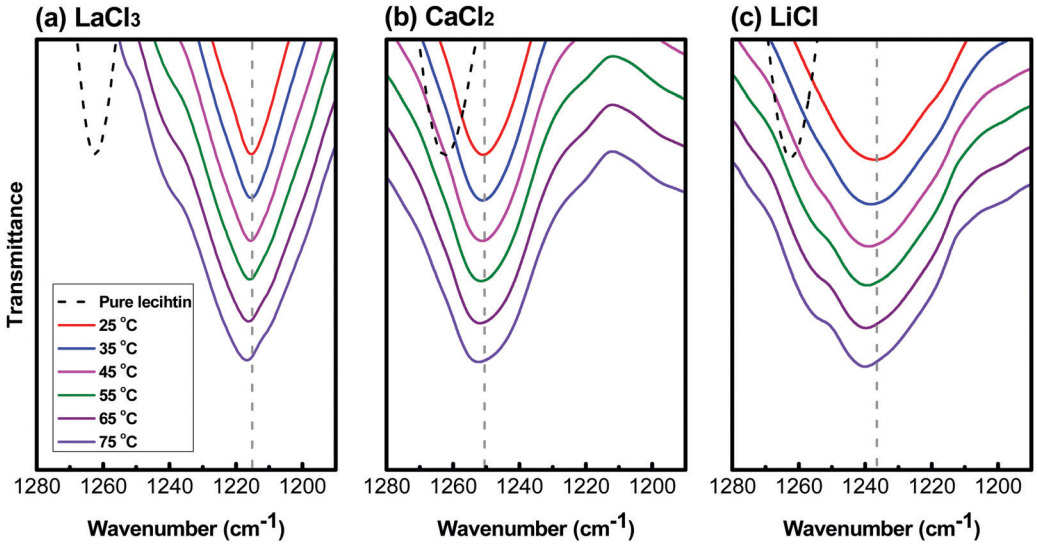

Fig. 6 FTIR absorption bands of phosphate on lecithin for lecithin/inorganic salt mixtures in *n*-decane at varying temperatures. The black dashed curves are the bands of pure lecithin at 25 °C.

of the temperature effect on the interactions, $\Delta\nu_{25\rightarrow75}$ is normalized by $\Delta\nu_{salt}$, and the $\Delta\nu_{25\rightarrow75}/\Delta\nu_{salt}$ values are 4.2%, 9.1%, and 16.0% for $LaCl_3$, $CaCl_2$, and LiCl, respectively. The values can be regarded as the degree of weakening for the interactions upon heating. In other words, FTIR confirms that the electrostatic interactions between lecithin and the high-valent cations are stronger and are less affected by temperature, consistent with the changes in G_p and the micellar structures as described in preceding sections.

3.4 Mechanisms

Different from the temperature-insensitive G_p of the wormlike micelles formed in water, we have shown that G_p of the lecithin organogels induced by inorganic salts through electrostatic interactions decreases with increasing temperature, analogous to the behaviors of the lecithin reverse worms induced by water or bile salts through hydrogen bonding, but with slower decay rates. The origins of the driving forces for the self-assembly of amphiphiles in water and in low-polar oils are different from the thermodynamic points of view. In water, the micellization is driven by the hydrophobic interaction that originates from an increase in water entropy upon formation of micelles. Such an entropic force gives rise to a peculiar response to temperature, that is, the hydrophobic interaction is getting stronger, not weaker, as the temperature increases, as evidenced by the increase of the critical micellization concentration (CMC).[7] Therefore, the predominant effect of temperature on the normal worms is simply the acceleration in the dynamics of surfactant exchange between micelles.[1] In low-polar oils, the driving forces for the micellization are the interactions between the hydrophilic headgroups of surfactants, typically the secondary bonds such as hydrogen bonding or electrostatic interactions that form in order to lower energy. The bonding energies of the weak interactions are comparable to thermal energy so that the strengths of the interactions are susceptible to temperature. Therefore, in addition to the accelerated dynamics of surfactant exchange, a reduced driving force for micellar growth comes into play for reverse worms as temperature is increased.

It has been shown that the growth of cylindrical micelles is caused by the excess free energy associated with the hemispherical end-caps compared to the cylindrical body of the worms (E_c in eqn (15)).[1] The more rapid exchange of surfactant unimers at a higher temperature weakens the influence of the unfavorable end-caps. As a result, more end-caps are formed, leading to shorter worms that in turn cause t_R and η_0 to decrease with increasing temperature. G_p is primarily proportional to the entanglement density of the worms. Although the worms become shorter upon heating, they are still sufficiently long to entangle and the entanglement density of the worms remains constant. This explains why G_p is constant with temperature for normal worms. In the case of the present reverse worms, the electrostatic attractions between the inorganic salts and lecithin headgroups are expected to weaken upon heating, which reduces the driving force for the growth of long reverse worms. Along with the effect of surfactant exchange, the length of the reverse worms decreases more rapidly than does the normal worms. This causes some worms to fall below a length sufficient for entanglement. The entanglement

Table 3 FTIR absorption bands (cm^{-1}) of phosphates on lecithin for lecithin/inorganic salt mixtures in *n*-decane at 25 °C and 75 °C

Salts	25 °C	75 °C	$\Delta\nu_{salt}$	$\Delta\nu_{25\rightarrow75}$	$\Delta\nu_{25\rightarrow75}/\Delta\nu_{salt}$
$LaCl_3$	1215	1217	47	2	4.2%
$CaCl_2$	1251	1252	11	1	9.1%
LiCl	1237	1241	25	4	16.0%

$\Delta\nu_{salt}$: redshift from pure lecithin to lecithin/inorganic salt mixtures at 25 °C. $\Delta\nu_{25\rightarrow75}$: blueshift from 25 to 75 °C for lecithin/inorganic salt mixtures.

Published on 02 March 2020. Downloaded by National Synchrotron Radiation Research on 1/27/2021 3:24:05 AM.

density of reverse worms would decrease and G_p thus drops with increasing temperature. Since the trivalent La^{3+} and divalent Ca^{2+} cations strongly interact with phosphates on lecithin, the electrostatic binding strength decays slower than does the monovalent Li^+ upon heating, as evidenced by FTIR. The lengths of the reverse worms induced by $LaCl_3$ and $CaCl_2$ are thus less sensitive to temperature, as revealed by SAXS. This explains the greater decrease in G_p for the reverse worms induced by LiCl.

4. Conclusions

In this study, we have correlated the temperature-dependent rheological properties with the strength of the electrostatic interaction that drives the formation of reverse wormlike micelles. Three inorganic salts with different electrostatic binding strengths with lecithin were used to induce reverse worms. We show that the decay of G_p with increasing temperature for the reverse worms driven by electrostatic interactions lies between the worms driven by hydrophobic interactions and hydrogen bonding, and a more rapid decay is found for the inorganic salt of weaker interaction with lecithin, consistent with the changes in the interaction strength determined by FTIR and the changes in the length of reverse worms determined by SAXS upon heating. The decrease in the plateau modulus for reverse worms is due to the weakening of the electrostatic interactions as the temperature is increased, which in turn causes a rapid decrease in the length of the reverse worms. The results presented here give insights into the mechanism for the formation of revere worms, and emphasize the thermodynamic origin and the strength of the interactions as the key factors that dictate the rheology of wormlike micelles.

Conflicts of interest

There are no conflicts of interest to declare.

Acknowledgements

This work was financially supported by the ''Advanced Research Center of Green Materials Science and Technology'' from the Featured Area Research Center Program within the framework of the Higher Education Sprout Project by the Ministry of Education (107L9006) and the Ministry of Science and Technology in Taiwan (MOST 106-2628-E-002-006-MY3, 107-3017-F-002-001, and 107-2622-8-006-015). The authors also acknowledge the National Synchrotron Radiation Research Center, Taiwan, for facilitating the X-ray scattering experiments.

References

1 M. E. Cates and S. J. Candau, *J. Phys.: Condens. Matter*, 1990, **2**, 6869–6892.
2 H. Hoffmann, in *Structure and Flow in Surfactant Solutions*, ed. C. A. Herb and R. K. Prud'homme, American Chemical Society, Washington, DC, 1994.
3 R. Scartazzini and P. L. Luisi, *J. Phys. Chem.*, 1988, **92**, 829–833.
4 P. Schurtenberger, R. Scartazzini and P. L. Luisi, *Rheol. Acta*, 1989, **28**, 372–381.
5 P. L. Luisi, R. Scartazzini, G. Haering and P. Schurtenberger, *Colloid Polym. Sci.*, 1990, **268**, 356–374.
6 P. Schurtenberger, L. J. Magid, S. M. King and P. Lindner, *J. Phys. Chem.*, 1991, **95**, 4173–4176.
7 D. F. Evans and H. Wennerstrom, *The Colloidal Domain: Where Physics, Chemistry, Biology, and Technology Meet*, Wiley-VCH, New York, 2001.
8 J. F. Berret, in *Molecular Gels: Materials with Self-Assebled Fibrillar Networks*, ed. P. Terech and R. G. Weiss, Springer, Dordrecht, The Netherlands, 2005.
9 N. V. Nucci and J. M. Vanderkooi, *J. Phys. Chem. B*, 2005, **109**, 18301–18309.
10 H. Akutsu and J. Seelig, *Biochemistry*, 1981, **20**, 7366–7373.
11 S.-H. Tung, Y.-E. Huang and S. R. Raghavan, *J. Am. Chem. Soc.*, 2006, **128**, 5751–5756.
12 S.-H. Tung, Y.-E. Huang and S. R. Raghavan, *Langmuir*, 2007, **23**, 372–376.
13 L. Sun, C. D. Wick, J. I. Siepmann and M. R. Schure, *J. Phys. Chem. B*, 2005, **109**, 15118–15125.
14 C.-Y. Cheng, H. Oh, T.-Y. Wang, S. R. Raghavan and S.-H. Tung, *Langmuir*, 2014, **30**, 10221–10230.
15 H.-Y. Lee, K. K. Diehn, S. W. Ko, S.-H. Tung and S. R. Raghavan, *Langmuir*, 2010, **26**, 13831–13838.
16 S.-T. Lin, C.-S. Lin, Y.-Y. Chang, A. E. Whitten, A. Sokolova, C.-M. Wu, V. A. Ivanov, A. R. Khokhlov and S.-H. Tung, *Langmuir*, 2016, **32**, 12166–12174.
17 J. R. Rydall and P. M. Macdonald, *Biochemistry*, 1992, **31**, 1092–1099.
18 J. Marra and J. Israelachvili, *Biochemistry*, 1985, **24**, 4608–4618.
19 R. J. Clarke and C. Lüpfert, *Biophys. J.*, 1999, **76**, 2614–2624.
20 J. J. Dannenberg, L. Haskamp and A. Masunov, *J. Phys. Chem. A*, 1999, **103**, 7083–7086.
21 U.-S. Jeng, C. H. Su, C.-J. Su, K.-F. Liao, W.-T. Chuang, Y.-H. Lai, J.-W. Chang, Y.-J. Chen, Y.-S. Huang, M.-T. Lee, K.-L. Yu, J.-M. Lin, D.-G. Liu, C.-F. Chang, C.-Y. Liu, C.-H. Chang and K. S. Liang, *J. Appl. Crystallogr.*, 2010, **43**, 110–121.
22 C. Dreiss, *Soft Matter*, 2007, **3**, 956–970.
23 A. Guinier, *Small-angle scattering of X-rays*, John Wiley & Sons, Ltd, New York, US, 1955.
24 S. Kline, *J. Appl. Crystallogr.*, 2006, **39**, 895–900.
25 J. S. Pedersen and P. Schurtenberger, *Macromolecules*, 1996, **29**, 7602–7612.
26 Y. A. Shchipunov, *Colloids Surf., A*, 2001, **183–185**, 541–554.
27 S. J. Candau, E. Hirsch, R. Zana and M. Delsanti, *Langmuir*, 1989, **5**, 1225–1229.
28 P. Fischer and H. Rehage, *Langmuir*, 1997, **13**, 7012–7020.

 This journal is © The Royal Society of Chemistry 2020

Published on 02 March 2020. Downloaded by National Synchrotron Radiation Research on 1/27/2021 3:24:05 AM.

29 D. Gaudino, R. Pasquino and N. Grizzuti, *J. Rheol.*, 2015, **59**, 1363–1375.
30 R. Granek and M. Cates, *J. Chem. Phys.*, 1992, **96**, 4758–4767.
31 A. Khatory, F. Lequeux, F. Kern and S. J. Candau, *Langmuir*, 1993, **9**, 1456–1464.
32 R. G. Larson, *J. Rheol.*, 2012, **56**, 1363–1374.
33 R. A. Böckmann and H. Grubmüller, *Angew. Chem., Int. Ed.*, 2004, **43**, 1021–1024.
34 U. R. Pedersen, C. Leidy, P. Westh and G. H. Peters, *Biochim. Biophys. Acta, Biomembr.*, 2006, **1758**, 573–582.
35 G. Pabst, A. Hodzic, J. Štrancar, S. Danner, M. Rappolt and P. Laggner, *Biophys. J.*, 2007, **93**, 2688–2696.